

Center for Quality and Applied Statistics
Kate Gleason College of Engineering
Rochester Institute of Technology

**Analytical Comparison of the Matched Filter
and Orthogonal Subspace Projection
Detectors in Structured Models for
Hyperspectral Images**

Peter Bajorski
Center for Quality and Applied Statistics
Rochester Institute of Technology
Peter.Bajorski@rit.edu

Technical Report 2005–7

September 2005



Analytical Comparison of the Matched Filter and Orthogonal Subspace Projection Detectors in Structured Models for Hyperspectral Images

Peter Bajorski

Graduate Statistics Department, Rochester Institute of Technology

98 Lomb Memorial Drive, Rochester, NY 14623-5604

Email: Peter.Bajorski@rit.edu

ABSTRACT

In this paper, we perform an analytical comparison of two well-known detectors—the matched filter detector (MFD) and the orthogonal subspace projection (OSP) detector for the subpixel target detection in hyperspectral images under the assumption of the structured model. The OSP detector (equivalent to the least squares estimator) is a popular detector utilizing background signature information. On the other hand, the MFD is intended for a model without background information, and it is often used for its simplicity. The OSP detector seems to be more reliable because it removes the interference of background signatures. However, it has been demonstrated in the literature that sometimes the MFD can be more powerful. In this paper, we show analytical results explaining the relationship between the two detectors beyond the anecdotal evidence from specific hyperspectral images or simulations. We also give some guidelines on when the MFD may be more beneficial than the OSP, and when the OSP is better because of being more robust against a wide range of conditions.

Keywords: target detection, structured model, hyperspectral image, matched filter, OSP, detection power.

I. INTRODUCTION

The purpose of this paper is to perform analytical comparisons of the matched filter detector (MFD) and the orthogonal subspace projection (OSP) detector that would at least partially explain the behavior of these detectors in real hyperspectral images. A traditional theoretical approach to target detection is to assume a certain probabilistic model and then use the appropriate detectors (test statistics) that have good properties under the assumed model. For example, the OSP detector (equivalent to the least squares estimator) seems to be a reasonable detector for the structured model (containing the target and background signatures) considered in this paper. On the other hand, the MFD is intended for a different model since it is equivalent to the least squares estimator in the structured model containing only the target signature. As such, it may seem that the MFD (using less information) would be inferior to the OSP. However, in practice, the MFD may sometimes outperform the OSP as demonstrated by simulations in [10] (although for the whitened versions of these detectors). Practitioners often use the MFD for its simplicity because it does not require the knowledge (or estimation) of the background signatures. So, it would be useful to have a better understanding of the relationship between the two detectors beyond the anecdotal evidence from specific hyperspectral images or simulations.

In this paper, we investigate properties of both detectors under the same conditions, that is, for the more general structured model with the background signatures. We show analytical results explaining when the MFD outperforms the OSP and when the opposite is true. We also give some guidelines on when the MFD may be more beneficial than the OSP, and when the OSP is better because of being more robust against a wide range of conditions.

In Section II, we formulate the model assumed in this paper. In Section III, we introduce the MFD and OSP detectors and also list many other detectors introduced in the literature that are equivalent to one of these two detectors. Most of the equivalencies of the detectors are already known in literature, but they are not always well known among practitioners. We also show one new equivalency result by proving explicitly that the detector termed the signature space orthogonal projection classifier (SSC) in [1] is equivalent to the OSP detector. The main results concerning the detection power of the MFD and OSP are shown in Section IV, and conclusions are drawn in Section V.

II. MODEL FORMULATION

For the purpose of subpixel target detection, the following structured model is often used in the literature ([1], [2], [3], [4], [5]):

$$\mathbf{r} = \mathbf{d} \cdot \theta + \mathbf{U} \cdot \boldsymbol{\gamma} + \boldsymbol{\varepsilon} \quad (1)$$

where \mathbf{r} is a p -dimensional vector (of reflectance or radiance, for example) of a pixel spectrum, \mathbf{d} is a fixed known vector of the target spectrum, \mathbf{U} is a fixed known matrix of background spectra as columns, and θ , $\boldsymbol{\gamma}$ are the unknown target scalar abundance and the vector of background abundances, respectively. The error term $\boldsymbol{\varepsilon}$ is assumed to follow the multivariate normal (Gaussian) distribution $N(\mathbf{0}, \sigma^2 \mathbf{I})$. The term $\boldsymbol{\varepsilon}$ represents the effect of the noise in data. The background spectra \mathbf{U} are sometimes called interference or undesired target spectra.

It should be emphasized that we do not explicitly assume the sum-to-one constraint that all abundances add up to 1 (or any stronger condition such as all non-negative abundances (except for non-negative target abundance)). We believe that such an additional constraint is desirable (based on the physical interpretation of abundances), but in some practical situations, it may not necessarily be strictly fulfilled. For example, when part of the pixel area is taken by low reflectance material (such as chalcopyrite shown later or carbon), it may not be identified as one of the background signatures in \mathbf{U} . Consequently, the sum of all abundances might be smaller than one. Other imperfections in the process of identifying the background signatures or in the assumption of perfect linearity in the mixing process may lead to negative abundances or their sum being larger than 1. So, the question is: when we see such imperfections, should we force the abundances to conform to the desirable constraints. Clearly, in the case of a missing low reflectance material, such procedures would lead to distortions in the estimation of the correct abundances.

This is not to say that we should not use the sum-to-one constraint. In this paper, most theoretical results and examples are discussed under the additional sum-to-one constraint. However, if we were to adhere strictly to the sum-to-one constraint, then instead of using the least-squares estimates such as the OSP, we should always use constrained least-squares estimates. As demonstrated in [12], the constrained signal detector (CSD) outperforms the OSP. One justification for using the OSP (which is still a popular choice) is that it is somewhat more general and may better address those imperfect situations.

The target detection problem is often defined in the literature as the hypothesis-testing problem for testing the null hypothesis $H_0 : \theta = 0$ versus the alternative hypothesis $H_1 : \theta > 0$. The abundance θ is assumed to be nonnegative according to its physical interpretation. At the same time, the background abundance vector $\boldsymbol{\gamma}$ might be different for the two hypotheses, which we emphasize in the following notation (with $\theta > 0$):

$$\begin{aligned} H_0 : \mathbf{r} &= \mathbf{U} \cdot \boldsymbol{\gamma}_0 + \boldsymbol{\varepsilon} \\ H_1 : \mathbf{r} &= \mathbf{d} \cdot \theta + \mathbf{U} \cdot \boldsymbol{\gamma}_1 + \boldsymbol{\varepsilon} \end{aligned} \tag{2}$$

III. DETECTORS

In this section, we discuss two detectors—the matched filter detector (MFD) and the orthogonal subspace projection (OSP) detector. We also point out that many other detectors are equivalent to these two detectors. In order to simplify the presentation, we will associate the word “detector” with one of the following (where the meaning will be clear from the context):

1. An operator $D : R^p \rightarrow R$.
2. A vector \mathbf{w} defining a linear operator $D : \mathbf{r} \mapsto \mathbf{w}^T \mathbf{r}$.
3. The value of the operator $D(\mathbf{r})$.
4. A decision procedure indicating presence of the target when $D(\mathbf{r}) > c$, and its absence otherwise.

We would like to stress that two detectors differing by a constant (both in an additive and multiplicative sense) are equivalent in the sense of the meaning 4 above. Let us assume that a detector $D(\mathbf{r})$ indicates the presence of the target when $D(\mathbf{r}) > c$, where c is an appropriately chosen constant (for example, to achieve a certain false alarm probability). We can define another detector $D'(\mathbf{r}) = a \cdot D(\mathbf{r}) + b$ indicating the presence of the target when $D'(\mathbf{r}) > c'$ for $a > 0$ (and $D'(\mathbf{r}) < c'$ for $a < 0$). Clearly, c' can be chosen as $a \cdot c + b$, so that both detectors have the same detection effect and the same properties. These statements form a sufficiently formal proof of equivalence, but a more elaborate proof is included in [4] (Section IV).

A. Matched filter detector (MFD)

The matched filter detector (MFD) operating on the image spectrum \mathbf{r} is defined as

$$D_{MFD}(\mathbf{r}) = \frac{\mathbf{d}^T \mathbf{r}}{\mathbf{d}^T \mathbf{d}} \quad (3)$$

The scaling of MFD is chosen so that $D_{MFD}(\mathbf{r})$ is an unbiased estimator of θ in the following reduced (relative to (1)) model

$$\mathbf{r} = \mathbf{d} \cdot \theta + \boldsymbol{\varepsilon} \quad (4)$$

Clearly, $D_{MFD}(\mathbf{r})$ is the same as the least squares (and maximum likelihood) estimator of θ in model (4) (see [11]).

However, we will see later on that $D_{MFD}(\mathbf{r})$ is usually a biased estimator of θ in the presence of the background in model (1).

B. Orthogonal subspace projection (OSP) detector

The orthogonal subspace projection (OSP) detector operating on the image spectrum \mathbf{r} is defined as

$$D_{OSP}(\mathbf{r}) = \frac{\mathbf{d}^T P_{\mathbf{U}}^{\perp} \mathbf{r}}{\mathbf{d}^T P_{\mathbf{U}}^{\perp} \mathbf{d}} \quad (5)$$

where $P_{\mathbf{U}}^{\perp} = \mathbf{I} - \mathbf{U}(\mathbf{U}^T \mathbf{U})^{-1} \mathbf{U}^T$ is a projection on the subspace orthogonal to \mathbf{U} . The OSP detector was introduced in [7] (with a different scaling), and further investigated in many publications (recently, for example, in [6] and [14]). The connection with the regular unmixing through the least squares was pointed out in [8], where the author writes that “it is not clear what advantages the use of OSP has over the direct application of spectral unmixing” (p. 1046). We agree that the two approaches are formally equivalent; however, there are some advantages of using the OSP notation (5). The reason for using the OSP name and notation here is twofold—the OSP name is now broadly used in the detection literature, and the OSP in (5) gives an explicit formula for the least squares estimator of θ , which is convenient for some analytical considerations.

The OSP is a special case of a matched subspace filter (see [3]). It is also the least squares (and maximum likelihood) estimator of θ in model (1) (see [8], [10], and Section VI.b in this paper). Table 1 shows some other equivalent forms of the OSP and MFD detectors.

There are also many other detectors discussed in the literature. For example, the constrained energy minimization (CEM) filter discussed in [15] and the target-constrained interference-minimized filter (TCIMF) presented in [16] turn out to be whitened versions of the MFD and OSP detectors (see [10]). Consequently, the results of this paper also apply to the CEM and TCIMF detectors after the appropriate corrections for whitening. More information about a wide range of subpixel target detectors can be found in references cited in this paper (especially in [2] and [6]). Also some other approaches to the model formulation are used in literature (in [17], for example).

IV. DETECTION POWER

Let us now discuss the relationship between hypothesis testing and practical target detection. In hypothesis testing, we need to know the distribution of $D(\mathbf{r})$ (under the null hypothesis) in order to find the constant c that would guarantee

a certain false alarm probability (probability of type I error). In practical target detection in spectral images, such distributions are usually not known, and at this point, there is no reliable method to find the appropriate constant c . So, practical target detection is based on calculating the values of $D(\mathbf{r})$ for all pixel spectra \mathbf{r} , and associating a certain number of highest values of $D(\mathbf{r})$ with detected targets. This is equivalent to considering certain values for c and then observing false alarm rates (as estimates of the false alarm probability) rather than calculating the desired c .

In the current target detection literature, we can identify three primary methods by which the detectors are evaluated:

- i. A stochastic model for the spectrum \mathbf{r} is assumed (similar to our model (1)), and the distribution of $D(\mathbf{r})$ is calculated, which leads to theoretical ROC curves (plots of probability of detection versus false alarm probabilities) and power curves (plots of detection power (probability of detection) versus a parameter measuring the departure from the null hypothesis (for example, the target abundance)).
- ii. An artificial set of pixel spectra is created with predetermined knowledge of target pixels. In this case, observed ROC curves (plots of detection rates versus false alarm rates) and observed power curves can be plotted. By the “rate,” we mean the relative frequency of an event (detection or false alarm) as opposed to its theoretical probability. When the set of pixel spectra is relatively small (for example, several hundred spectra as in [1] and [5]), the results resemble those for the real images, that is, statements are made about the number of pixels identified as containing the target, or simply detector values are reported. When the set of pixel spectra is very large (for example, several thousand spectra as in [10]) and appropriately constructed, the results can be regarded as simulated approximations of the theoretical values (such as those calculated in the first type of study).
- iii. A real spectral image is used, where the location of the target pixels is known. In this case, we also use observed ROC curves, while the observed power curves are not usually practical because it is unlikely to find a sufficient number of pixels with similar departures from the null hypothesis. For the same reason, the observed ROC curves are not as “clean” as those constructed in the first type of study because the target pixels are usually not homogeneous enough, that is, they may contain varying amounts of background materials.

In the study type (iii), the constant c is not calculated, but instead, by changing its value, we observe a range of false alarm rates and resulting detection rates. The study type (i) resembles the statistical hypothesis testing situation, where the constant c is calculated, while the study type (iii) is somewhat different because we do not necessarily need to calculate c . This point is further explored in this section.

We now want to compare the two detectors, MFD and OSP, under the assumption of model (1). It is a well-known result in linear models and target detection literature, that under the assumptions of model (1), the OSP statistic (5) follows the normal distribution $N\left(\theta, \left(\mathbf{d}^T P_U^\perp \mathbf{d}\right)^{-1} \sigma^2\right)$. The situation is slightly more complex when model (1) is true, but we perform target detection without using the background signatures \mathbf{U} , that is, we act as if model (4) were correct. In such a case, we would use the MFD detector given by (3). According to the theory of linear models ([11]), the MFD statistic (3) follows the normal (Gaussian) distribution

$$D_{MFD}(\mathbf{r}) \sim N\left(\theta + \mathbf{a}^T \boldsymbol{\gamma}, \left(\mathbf{d}^T \mathbf{d}\right)^{-1} \sigma^2\right) \quad (6)$$

under the assumptions of model (1), where $\mathbf{a}^T = \left(\mathbf{d}^T \mathbf{d}\right)^{-1} \mathbf{d}^T \mathbf{U}$. The same result was obtained in [1] (but in a more complex form) for the TSC detector (equivalent to MFD) and then was simplified in [4]. This result means that the MFD statistic is a biased estimator of θ under model (1) when $\mathbf{a}^T \boldsymbol{\gamma} \neq 0$. Since under the null hypothesis H_0 in (2)

$$D_{MFD}(\mathbf{r}) \stackrel{H_0}{\sim} N\left(\mathbf{a}^T \boldsymbol{\gamma}_0, \left(\mathbf{d}^T \mathbf{d}\right)^{-1} \sigma^2\right),$$

the decision procedure $D_{MFD}(\mathbf{r}) > c$ achieves the probability of a false alarm α when $c = c_{MFD} = \mathbf{a}^T \boldsymbol{\gamma}_0 + \left(\mathbf{d}^T \mathbf{d}\right)^{-1/2} \sigma \cdot z_{1-\alpha}$, where $z_{1-\alpha}$ is the $(1-\alpha)$ percentile from the standard normal (Gaussian) distribution. Since the constant vector of abundances $\boldsymbol{\gamma}_0$ is unknown, we cannot find the appropriate constant c such that the decision procedure $D_{MFD}(\mathbf{r}) > c$ would achieve a specified probability of false alarm. However, in practical target detection, we do not really calculate c but rather associate the highest values of $D_{MFD}(\mathbf{r})$ with pixels containing the target, as explained at the beginning of this section. This approach is equivalent to trying different

values of c and observing the properties of the decision procedure $D_{MFD}(\mathbf{r}) > c$. We will use the same approach here.

This also explains why we can use both the MFD and OSP detectors without knowing σ .

Using the above calculated value of c_{MFD} and property (6) for $\gamma = \gamma_1$, we obtain the following formula for the detection power of the MFD

$$P_{MFD,\alpha} = 1 - \Phi \left(z_{1-\alpha} - \frac{\sqrt{\mathbf{d}^T \mathbf{d}}}{\sigma} [\theta + \mathbf{a}^T (\gamma_1 - \gamma_0)] \right) \quad (7)$$

where Φ is the cumulative distribution function of the standard normal (Gaussian) distribution. Similar calculations for the OSP lead to the following formula for its detection power

$$P_{OSP,\alpha} = 1 - \Phi \left(z_{1-\alpha} - \frac{\theta}{\sigma} \sqrt{\mathbf{d}^T P_{\mathbf{U}}^{\perp} \mathbf{d}} \right) \quad (8)$$

In order to simplify the analysis of detection power, we introduce the following notation:

$$B = \frac{\|\mathbf{d}\theta\|}{\sigma} = \frac{\theta}{\sigma} \sqrt{\mathbf{d}^T \mathbf{d}}$$

and ω is the angle between \mathbf{d} and the subspace $\langle \mathbf{U} \rangle$ generated by column vectors of \mathbf{U} ($0^\circ \leq \omega \leq 90^\circ$). That is,

$$\sin(\omega) = \frac{\sqrt{\mathbf{d}^T P_{\mathbf{U}}^{\perp} \mathbf{d}}}{\sqrt{\mathbf{d}^T \mathbf{d}}}.$$

In practice, $\omega \neq 0^\circ$ because \mathbf{d} is linearly independent of \mathbf{U} , and usually $\omega \neq 90^\circ$ because two spectra (vectors of non-negative values) are never orthogonal except in some unrealistic cases. The angle ω could sometimes be 90° if the spectra \mathbf{r} were mean-centered, but this is not considered in this paper. So, for the purpose of this paper, we will assume that $0^\circ < \omega < 90^\circ$. The parameter B can be regarded as a signal to noise ratio (SNR) for the signal $\mathbf{d}\theta$. The detection power of both detectors can now be expressed as

$$P_{MFD,\alpha} = 1 - \Phi(z_{1-\alpha} - \Delta_{MFD}) \quad (9)$$

$$P_{OSP,\alpha} = 1 - \Phi(z_{1-\alpha} - \Delta_{OSP}) \quad (10)$$

where $\Delta_{MFD} = B \left[1 + \frac{\mathbf{a}^T (\boldsymbol{\gamma}_1 - \boldsymbol{\gamma}_0)}{\theta} \right]$ and $\Delta_{OSP} = B \sin(\omega)$. We also define the efficiency of MFD versus OSP as

$$Eff(MFD, OSP) = \frac{\Delta_{MFD}}{\Delta_{OSP}} = \frac{1 + \frac{\mathbf{a}^T (\boldsymbol{\gamma}_1 - \boldsymbol{\gamma}_0)}{\theta}}{\sin(\omega)} \quad (11)$$

Since Δ_{OSP} is always positive (for $0^\circ < \omega < 90^\circ$), we can say that the MFD has power larger than the OSP when $Eff(MFD, OSP) > 1$, and the OSP is more powerful when $Eff(MFD, OSP) < 1$. Additionally, negative Δ_{MFD} (and consequently negative $Eff(MFD, OSP)$) indicates a very poor performance of MFD with $P_{MFD,\alpha} < \alpha$. On the other hand, non-negative $\mathbf{a}^T (\boldsymbol{\gamma}_1 - \boldsymbol{\gamma}_0)$ is very beneficial to MFD as shown by Theorem 1 below. Some examples of non-negative $\mathbf{a}^T (\boldsymbol{\gamma}_1 - \boldsymbol{\gamma}_0)$ are shown later on in subsections B and C.

Theorem 1. Under the hypotheses (2) and the previous natural assumption that $0^\circ < \omega < 90^\circ$, the condition $\mathbf{a}^T (\boldsymbol{\gamma}_1 - \boldsymbol{\gamma}_0) \geq 0$ implies that

$$P_{OSP,\alpha} < P_{MFD,\alpha} \quad (12)$$

for $\alpha \in (0, 1)$.

Proof. This theorem is an obvious conclusion from (11) and from the theorem assumptions. \square

Even though the MFD detection power depends (in general) on the abundances of the background materials, we are sometimes able to obtain useful boundaries that will tell us that the power is sufficiently large. To this end, the following theorem is helpful.

Theorem 2. Under the hypotheses (2), and the fully constrained case ($\theta + \sum_i \gamma_{1,i} = 1$, $\sum_i \gamma_{0,i} = 1$, where $\gamma_{1,i}$ and $\gamma_{0,i}$ are non-negative coordinates of the vectors $\boldsymbol{\gamma}_1$ and $\boldsymbol{\gamma}_0$, respectively),

$$\min_{\gamma_1, \gamma_0} P_{MFD, \alpha} = 1 - \Phi \left(z_{1-\alpha} - \frac{\sqrt{\mathbf{d}^T \mathbf{d}}}{\sigma} \left[\theta - \max_i a_i + (1-\theta) \min_i a_i \right] \right) \quad (13)$$

for $\alpha \in (0,1)$, where a_i 's are coordinates of the vector \mathbf{a} .

Proof: Based on formula (7), we need to find the minimum of $\mathbf{a}^T (\gamma_1 - \gamma_0)$. Let k and m be such that $\max_i a_i = a_k$ and $\min_i a_i = a_m$. The term $\mathbf{a}^T (\gamma_1 - \gamma_0)$ is minimized when $\mathbf{a}^T \gamma_1$ is as small as possible and $\mathbf{a}^T \gamma_0$ is as large as possible (\mathbf{a} is constant and γ_1, γ_0 are independent of each other). Due to the sum-to-one constraint, $\mathbf{a}^T \gamma_1$ is the smallest when $\gamma_{1,m} = 1 - \theta$ and the remaining coordinates of γ_1 are zero. In the same fashion, $\mathbf{a}^T \gamma_0$ is the largest when $\gamma_{0,k} = 1$ and the remaining coordinates of γ_0 are zero. Finally, some straightforward algebra leads to the right-hand side of (13). \square

Theorem 2 is especially useful when the right-hand side of (13) leads to reasonably large values. This means that we can ensure a large power of the MFD for any combination of the background abundances γ_1 and γ_0 . An example of this will be shown in Example 4 (Subsection B). On the other hand, when the right-hand side of (13) leads to very small values (for example, below α), it means that we are not able to ensure reasonable MFD power uniformly over the range of background abundances. An example of this type of situation is shown in Example 3 (Subsection B).

We now consider several scenarios for a more detailed comparison of the detection power of both detectors.

A. One-Dimensional Background

We now assume that

1. The matrix \mathbf{U} consists of only one background signature \mathbf{u}_1 (consequently γ is now a scalar)
2. The abundance coefficients sum up to 1, that is, $\gamma_0 = 1$ and $\theta + \gamma_1 = 1$

This case is sometimes called “uniform background” (see [12]) because the background is always the same material, and it is partially replaced by the target in some pixels. From the second assumption, we have $\gamma_1 - \gamma_0 = -\theta$. Now, the

vector \mathbf{a} becomes a scalar $a = \frac{\sqrt{\mathbf{u}_1^T \mathbf{u}_1}}{\sqrt{\mathbf{d}^T \mathbf{d}}} \cos(\omega) = \frac{\cos(\omega)}{SBR(\mathbf{d}, \mathbf{u}_1)}$, where we define $SBR(\mathbf{d}, \mathbf{u}_1)$ as the Signal to

Background Ratio according to the formula

$$SBR(\mathbf{d}, \mathbf{u}_1) = \frac{\sqrt{\mathbf{d}^T \mathbf{d}}}{\sqrt{\mathbf{u}_1^T \mathbf{u}_1}} \quad (14)$$

Finally,

$$\Delta_{MFD} = B \left[1 - \frac{\cos(\omega)}{SBR(\mathbf{d}, \mathbf{u}_1)} \right] \quad (15)$$

Theorem 3. Under the hypotheses (2), the assumptions 1 and 2 of this section, and the previous natural assumption that $0^\circ < \omega < 90^\circ$,

$$P_{OSP, \alpha} \leq P_{MFD, \alpha} \quad (16)$$

for $\alpha \in (0, 1)$, if and only if

$$SBR(\mathbf{d}, \mathbf{u}_1) \geq \frac{1 + \sin(\omega)}{\cos(\omega)} \quad (17)$$

and the equality holds in (16) if and only if the equality holds in (17).

Proof: From (9), (10), and (15), the inequality (16) is equivalent to $1 - \frac{\cos(\omega)}{SBR(\mathbf{d}, \mathbf{u}_1)} \geq \sin(\omega)$, which leads to

$$SBR(\mathbf{d}, \mathbf{u}_1) \geq \frac{\cos(\omega)}{1 - \sin(\omega)} = \frac{1 + \sin(\omega)}{\cos(\omega)} \text{ for } 0^\circ < \omega < 90^\circ. \quad \square$$

The inequality (17) shows explicitly when the MFD outperforms the OSP (or vice versa) depending on the Signal to Background Ratio $SBR(\mathbf{d}, \mathbf{u}_1)$ and the angle ω between the target and the background. The border line (that is, when the power of both detectors is the same) is shown in Figure 1 in the system of coordinates of $SBR(\mathbf{d}, \mathbf{u}_1)$ on the vertical axis and the angle ω on the horizontal axis. For the cases above the line, the MFD performs better than the OSP, and for those below the line, the OSP performs better.

Corollary 1. Under the assumptions of Theorem 2, the OSP always outperforms MFD, when $SBR(\mathbf{d}, \mathbf{u}_1) \leq 1$.

Proof: The function $\frac{1 + \sin(\omega)}{\cos(\omega)}$ is strictly increasing for $0^\circ \leq \omega < 90^\circ$, so $\frac{1 + \sin(\omega)}{\cos(\omega)} > \frac{1 + \sin(0)}{\cos(0)} = 1 \geq SBR(\mathbf{d}, \mathbf{u}_1)$

for $0^\circ < \omega < 90^\circ$, and from Theorem 2, we conclude that $P_{OSP,\alpha} > P_{MFD,\alpha}$ for $\alpha \in (0,1)$. \square

The above corollary tells us that when the target signal is weaker than the background signal, the OSP is a better detector. Figure 1 shows that for the large values of the angle ω (close to 90°), the OSP is also usually better unless the target signal is very strong. These results confirm the general understanding that the MFD might be better in some easier cases of subpixel target detection with easily visible targets, but the OSP may outperform the MFD in the more difficult cases when it is important to use the background information.

We now want to show two numerical examples with specific material spectra used in literature.

Example 1. The five spectral signatures used in Table 2 were intensively used in papers (for example, [1]) and in a recent book [6]. The spectra are shown in Figure 1.5 of the book [6]. The purpose of Table 2 is to show typical values of $SBR(\mathbf{d}, \mathbf{u}_1)$ and ω . The top triangle part above the main diagonal of Table 2 shows values of ω when one of the signatures is used as \mathbf{d} and one of the remaining four signatures is used as \mathbf{u}_1 . The maximum angle observed in Table 2 is below 33° , and some values are much lower. The bottom triangle part below the main diagonal of Table 2 shows values of $SBR(\mathbf{d}, \mathbf{u}_1)$ when the row material is used as \mathbf{d} and column material is used as \mathbf{u}_1 . The signal to background ratio SBR for the other half of the table can be calculated as the inverse values of the $SBR(\mathbf{d}, \mathbf{u}_1)$ values shown by using the obvious property: $SBR(\mathbf{x}, \mathbf{y}) = SBR(\mathbf{y}, \mathbf{x})^{-1}$. For ω below 33° , $SBR(\mathbf{d}, \mathbf{u}_1) \geq 1.85$ would ensure dominance of MFD over OSP. However, most $SBR(\mathbf{d}, \mathbf{u}_1)$ values in Table 2 are smaller than 1.85. To pinpoint the precise relationship between the OSP and MFD, Table 3 shows the $Eff(MFD, OSP)$ values of the efficiency of MFD versus OSP defined in (11) and calculated according to the formula

$$Eff(MFD, OSP) = \frac{1 - \frac{\cos(\omega)}{SBR(\mathbf{d}, \mathbf{u}_1)}}{\sin(\omega)} \quad (18)$$

Most of the values in Table 3 are below 1, showing the dominance of the OSP, with many negative values indicating extremely poor performance of MFD ($P_{MFD,\alpha} < \alpha$). Table 3 is convenient in summarizing many possible choices for the target and background spectra. However, it does not tell us specific values of detection power, which depends on several other factors.

Figure 2 shows detection power for the two detectors when the dry grass spectrum is the target \mathbf{d} and the creosote leaves spectrum is the background \mathbf{u}_1 . The false alarm rate α is assumed to be 0.001 because we are mostly interested in low false alarm rates. The SNR parameter B ranges from 0 to $\sqrt{10^{2.5}} \approx 17.78$, which is equivalent to θ ranging between 0 and 1, when the noise level σ is such that $\frac{\sqrt{\mathbf{d}^T \mathbf{d}}}{\sigma} = \sqrt{10^{2.5}}$ (that is, $\frac{\mathbf{d}^T \mathbf{d}}{\sigma^2}$ equal to 25 dB, which is considered for example in [10]). If the noise level is lower (that is, $\frac{\sqrt{\mathbf{d}^T \mathbf{d}}}{\sigma} > \sqrt{10^{2.5}}$), then Figure 2 covers a narrower range of values for θ . If the noise level is higher, then a certain left-hand-side fraction of Figure 2 covers the whole range of θ between 0 and 1. In this sense, Figure 2 is somewhat independent of the specific noise level assumed. In Figure 2, the performance of the OSP is only slightly better than that of the MFD, which is consistent with the value of $Eff(MFD, OSP) = 0.93$ from Table 3.

Figure 3 shows the case when the red soil spectrum is the target \mathbf{d} (while the background is still the creosote leaves spectrum) in a fashion similar to that of Figure 2. This time, the performance of the OSP is much better than that of the MFD, which is again consistent with the value of $Eff(MFD, OSP) = 0.49$ from Table 3.

We draw the following conclusions from Example 1 when a one-dimensional background is used. The blackbrush spectrum with low reflectance values can be much more easily detected when using the OSP, with almost no chance of detection with the MFD ($P_{MFD,\alpha} < \alpha$ because of the negative efficiency in Table 3). For detecting creosote leaves, the OSP is also much better unless it is on the blackbrush background. Dry grass has the highest overall reflectance (as

measured by $\sqrt{\mathbf{d}^T \mathbf{d}}$, and can usually be more easily detected by the MFD with the exception of the creosote leaves background, where the OSP is slightly better (due to a relatively large angle between the two materials). When blackbrush is the background material, any of the remaining materials can be more easily detected by the MFD.

Example 2. We now show some numerical results for the three material spectra used in [10]. The three reflectance spectra representing barite, chalcopyrite, and pyrite were downloaded from the USGS spectroscopy lab (see the appendix Section VI.c for details). The format of Table 4 is similar to that of Table 2, with values of the ω angle above the main diagonal and $SBR(\mathbf{d}, \mathbf{u}_1)$ below the main diagonal. Finally, Table 5 shows the $Eff(MFD, OSP)$ values in a format similar to that of Table 3. When barite is used as the target, the MFD dominates the OSP because the barite spectral curve is much higher than the spectral curves of the other two materials, and the ω angles are quite small. On the other hand, when barite is the background material, the MFD performs very poorly ($P_{MFD, \alpha} < \alpha$).

Figure 4 shows the case when the pyrite spectrum is used as the target \mathbf{d} , while the chalcopyrite spectrum is used as the background \mathbf{u}_1 in a fashion similar to that of Figures 2 and 3. This time the MFD is much better than the OSP, which is again consistent with the value of $Eff(MFD, OSP) = 2.01$ from Table 5. When barite is used as the target spectrum (as in [10]), the dominance of the MFD is even stronger.

In this example, we conclude that higher [or lower] overall reflectance of the target (as measured by $\sqrt{\mathbf{d}^T \mathbf{d}}$) was a deciding factor in the dominance of the MFD [or OSP] because the angles among the materials were quite small.

B. Two-Dimensional Background

We now assume that

1. The matrix \mathbf{U} consists of exactly two background signatures
2. The abundance coefficients are non-negative and sum up to 1

and we introduce the following notation: $\mathbf{a} = [a_1, a_2]^T$, $\boldsymbol{\gamma}_0 = [s, 1-s]^T$, $\boldsymbol{\gamma}_1 = [t, 1-t-\theta]^T$, where $0 \leq s \leq 1$ and $0 \leq t \leq 1-\theta$. It is easy to see that $\mathbf{a}^T(\boldsymbol{\gamma}_1 - \boldsymbol{\gamma}_0) = (t-s)(a_1 - a_2) - \theta a_2$. In an unlikely case when $a_1 = a_2$,

$\text{Eff}(MFD, OSP) = \frac{1-a_2}{\sin(\omega)}$, which does not depend on s and t (so one of the detectors is consistently dominant for all

choices of abundances). In the remaining part of this section, we assume that $a_1 \neq a_2$. Without loss of generality, we can assume that

3. $a_1 > a_2$.

Some straightforward algebra leads to the following two lemmas and a corollary under the assumptions 1-3 of this section.

Lemma 1. $\mathbf{a}^T(\boldsymbol{\gamma}_1 - \boldsymbol{\gamma}_0) \geq 0$ if and only if $t \geq s + \frac{\theta a_2}{a_1 - a_2}$.

Lemma 2. $\text{Eff}(MFD, OSP) \geq 1$ if and only if $t \geq s + \frac{\theta(\sin(\omega) - 1 + a_2)}{a_1 - a_2}$.

Corollary 2 (from Theorem 2). For any choice of $0 \leq s \leq 1$ and $0 \leq t \leq 1-\theta$,

$$P_{MFD, \alpha} \geq 1 - \Phi \left(z_{1-\alpha} - \frac{\sqrt{\mathbf{d}^T \mathbf{d}}}{\sigma} [\theta(1-a_2) - (a_1 - a_2)] \right) \quad (19)$$

Proof: This corollary can be concluded from Theorem 2 or proved directly as follows. Since $(a_1 - a_2)$ is positive, the expression $\mathbf{a}^T(\boldsymbol{\gamma}_1 - \boldsymbol{\gamma}_0) = (t-s)(a_1 - a_2) - \theta a_2$ takes on the smallest value for $t=0$ and $s=1$. Hence, formula (7) leads to (19). \square

Example 3. This example uses the same three reflectance spectra representing barite, chalcopyrite, and pyrite used in Example 2. The pyrite spectrum will represent the target \mathbf{d} , while barite and chalcopyrite spectra form the background

matrix \mathbf{U} . In this case, $\frac{a_2}{a_1 - a_2} \approx 0.1015$ and $\frac{(\sin(\omega) - 1 + a_2)}{a_1 - a_2} \approx 0.0992$. From Lemma 1, we conclude that

$\mathbf{a}^T(\boldsymbol{\gamma}_1 - \boldsymbol{\gamma}_0) \geq 0$ for any choice of (s, t) within the triangle $T_1 = \{(s, t) : 0 \leq s \leq 1 - 1.1015\theta, s + 0.1015\theta \leq t \leq 1 - \theta\}$,

which is a non-empty set for positive $\theta < (1.1015)^{-1} \approx 0.9$. This shows an example when the assumptions of Theorem 1 are fulfilled (and consequently the MFD outperforms the OSP). Based on Lemma 2, the MFD outperforms the OSP for any choice of (s, t) within a triangle $T_2 = \{(s, t) : 0 \leq s \leq 1 - 1.0992\theta, s + 0.0992\theta \leq t \leq 1 - \theta\}$, which is only slightly larger than T_1 .

We now continue with Example 3 and investigate specific values of detection power of both detectors. Clearly, the detection power of the OSP does not depend on (s, t) . On the other hand, the detection power of the MFD highly depends on (s, t) . Numerical results show that inside of the T_1 triangle the power of the MFD is almost 1, and then it rapidly decreases around the boundary of the T_2 triangle (which is only slightly larger than T_1 , as mentioned previously) along the line $t = s + 0.0992\theta$, and finally reaches values close to 0 outside of the T_2 triangle. This indicates that the use of the MFD may be beneficial for certain configurations of the background abundances, but the MFD may perform very poorly for some other configurations. For more specifics, let us assume the noise level σ is

such that $\frac{\sqrt{\mathbf{d}^T \mathbf{d}}}{\sigma} = \sqrt{10^{2.5}}$ and $\alpha = 0.001$. Even at $\theta = 0.9$, the detection power of the OSP is only 0.13, while for

$\theta = 0.1$, the OSP power is 0.002. Figure 5 shows the cross-sections of the MFD detection power for $\theta = 0.1$ as a function of the abundance s at various levels of t . The first (solid) line on the left-hand side is for $t = 0.1$, and the subsequent lines are for t increasing by 0.1 until the last line (function) on the right-hand side for $t = 0.9$. We can observe rapid changes from the very large power (almost 1) for smaller values of s to the very small power (almost 0) for larger values of s . This rapid change is happening in the vicinity of the boundary line $t = s + 0.0992\theta$ as mentioned before.

It is interesting to notice that the right-hand side of (19) is always smaller than α for the data in Example 3. This means that we are not able to ensure a reasonably large detection power of MFD in a uniform fashion for all background abundances, which is consistent with our observations from Figure 5.

Overall, we conclude that in the type of situation described in Example 3, it might be beneficial to use the MFD, especially when looking for targets taking only a relatively small fraction of a pixel (small θ), when t is significantly larger than s . However, the question is how can we know in practice that $t > s$. Here is one possible scenario. When we expect two possible materials in the background, we can calculate a_1 and a_2 . Let's assume that $a_1 > a_2$. For example, the first material may have much higher reflectance as in our case with barite. If we expect that first material (let's say barite) to be present together with the target material (pixels following the alternative hypothesis H_1) rather than on its own (pixels following the null hypothesis H_0), then chances are that $t > s$ and the MFD might be better. Otherwise, the OSP may be a more reliable detector.

Example 4. This example uses the same three reflectance spectra representing barite, chalcopyrite, and pyrite used in Example 3. This time, the barite spectrum will represent the target \mathbf{d} , while pyrite and chalcopyrite spectra form the background matrix \mathbf{U} . Figure 6 shows the detection power of the OSP (solid line) and the lower limit of the MFD power (dashed line), that is, the right-hand side of (19), as functions of the parameter θ . This means that for any (s, t) combination, the MFD power is above the dashed line, which shows performance much better than that of the OSP.

Figure 6 is plotted for $\frac{\sqrt{\mathbf{d}^T \mathbf{d}}}{\sigma} = \sqrt{10^{2.5}}$; however, it is independent of the specific noise level σ in the sense explained in the context of Figure 2. It is worthwhile to mention that based on Corollary 2, one can show that the lower limit of the MFD power is larger than the detection power of the OSP if and only if

$$\theta > \frac{a_1 - a_2}{1 - a_2 - \sin(\omega)}$$

and $1 - a_2 - \sin(\omega) > 0$. In our case $1 - a_2 - \sin(\omega) \approx 0.788$ and $\frac{a_1 - a_2}{1 - a_2 - \sin(\omega)} \approx 0.0846$. This means that for small θ

(<0.0846) the OSP power curve is actually above the lower limit of the MFD power, but it is not significant from a practical point of view because both powers are very small in that case.

C. Constant Background

In this section, we assume that $\gamma_1 = \gamma_0$. Clearly, this is not possible under the sum-to-one constraint. However, as we pointed out in Section II, this constraint may not always be fulfilled perfectly. We agree that $\gamma_1 = \gamma_0$ is not likely to happen in practice, but it can be regarded as an approximation of a situation when the background is constant in the sense of being the same mixture of background materials whether or not the target is present (in a special case, it could also be one material with a constant abundance). When the target is present, it does not replace any other material, perhaps because of some imperfections such as those discussed in Section II. In the case of a one-dimensional background, $\gamma_1 = \gamma_0$ is more likely to happen (or be a good approximation) when θ is very small. For a two-dimensional background, it can also be considered as an approximation when θ is very small and $t = s$.

Clearly, when $\gamma_1 = \gamma_0$, then $\mathbf{a}^T(\gamma_1 - \gamma_0) = 0$ and the MFD dominates the OSP under the remaining assumptions of Theorem 1.

D. Multi-dimensional Background

Based on Theorem 2, the type of the analysis performed in Example 4 can also be applied to backgrounds with a larger than 2 number of material spectra. For example, if some additional background materials were added such that the a_i coordinates of the vector \mathbf{a} for those materials were between the two numbers, $a_1 = 0.158$ for pyrite and $a_2 = 0.091$ for chalcopyrite, then the dashed line in Figure 6 would still represent the lower limit of the MFD power (the OSP power would get smaller because the angle ω would get smaller).

If all a_i 's were exactly the same (which is of course unlikely), then the MFD power would not depend on γ_1 and γ_0 ,

and $Eff(MFD, OSP) = \frac{1 - a_1}{\sin(\omega)}$, which is a generalization of a similar statement at the beginning of Subsection B.

V. CONCLUSIONS

The results obtained in this paper allow us to understand why and in what situations the MFD and OSP detectors may or may not work well. Theorem 1 shows a condition under which the MFD outperforms the OSP. It is then demonstrated in Example 3 that this condition may hold for a relatively broad range of the background abundances. Theorem 2 gives the lower limit of the MFD, which is then utilized in Example 4 to show a consistently large power of the MFD, when at the same time the OSP power is very small. In Subsection IV.A., we discuss the case of a one-dimensional background (also called a uniform background) and show exact conditions under which the OSP outperforms the MFD or vice versa. When the target signal is weaker than the background signal, then the OSP is a better detector (see Corollary 1). Only when the target signal is sufficiently strong (above the line shown in Figure 1), does the MFD become more powerful. The larger ω angle between the target and the background works in favor of the OSP with respect to the MFD (although both detectors are more powerful for larger ω angles). Specific numerical comparisons are performed in Examples 1 and 2.

Subsection IV.B. discusses the case of the two-dimensional background. Here the situation is more complex because the power of the MFD may vary depending on the background abundances. In Example 4, where the target signal is very strong as compared to the background spectra, the OSP power is very low, while the MFD power is quite large for sufficiently large θ . In this case, we can certainly recommend the MFD as a better detector. On the other hand, the use of the MFD is risky in the type of situation described in Example 3, because the MFD power might be very small for certain values of the background abundances (although it can also be very large for some other values of abundances). In Example 3, we discuss a scenario when some additional information about the observed materials may help in reducing that risk. In Subsection IV.D., we show that some of the conclusions from the two-dimensional background can also be extended to backgrounds with more signatures.

Overall, we conclude that in many situations it is possible to decide which of the two detectors, the OSP or the MFD, should be used based on the target and background signatures. For sufficiently strong target signals, the MFD tends to be the detector of choice within the examples analyzed in this paper. On the other hand, for many other cases, the OSP may be a more reliable choice with the detection power independent of the background abundances.

VI. APPENDIX

A. Oblique projections

Assume that \mathbf{H} and \mathbf{S} are $p \times m$ and $p \times k$ full rank matrices, respectively, the composite $p \times (m+k)$ matrix $\mathbf{M} = [\mathbf{H} \ \mathbf{S}]$ has also full rank, and $m+k \leq p$. Denote by $\langle \mathbf{H} \rangle$ a linear subspace generated by columns of \mathbf{H} . Based on our assumptions, the linear subspaces $\langle \mathbf{H} \rangle$ and $\langle \mathbf{S} \rangle$ are linearly independent but not necessarily orthogonal. The oblique projection is an idempotent linear operator $E_{\mathbf{HS}}$ (that is, $(E_{\mathbf{HS}})^2 = E_{\mathbf{HS}}$) whose range is $\langle \mathbf{H} \rangle$ and whose null space is $\langle \mathbf{S} \rangle$. It can be shown that

$$P_{\mathbf{M}} = E_{\mathbf{HS}} + E_{\mathbf{SH}} \quad (20)$$

which is easy to see geometrically or can also be concluded from identity (20) in [9]. In the same paper [9], it is shown that

$$E_{\mathbf{HS}} = \mathbf{H} \left(\mathbf{H}^T P_{\mathbf{S}}^{\perp} \mathbf{H} \right)^{-1} \mathbf{H}^T P_{\mathbf{S}}^{\perp} \quad (21)$$

B. Equivalency of Detectors

In this section, we give more details and some derivations related to the equivalency of detectors as described in Table 1. It is known that the least squares estimates are obtained through an orthogonal projection onto the subspace generated by the deterministic part of the model (1), that is,

$$P_{\mathbf{M}} \mathbf{r} = \mathbf{d} \cdot \hat{\theta}_{LS} + \mathbf{U} \cdot \hat{\gamma}_{LS} \quad (22)$$

where $\mathbf{M} = [\mathbf{d} \ \mathbf{U}]$ is the composite matrix consisting of \mathbf{d} and all columns of \mathbf{U} . The least squares estimator $\hat{\theta}_{LS}$ of θ in the model (1) can also be associated with the oblique projection, that is (see [9]):

$$\mathbf{d} \cdot \hat{\theta}_{LS} = E_{\mathbf{d}\mathbf{U}} \mathbf{r}$$

which leads to

$$\mathbf{d}^T \mathbf{d} \cdot \hat{\theta}_{LS} = \mathbf{d}^T E_{\mathbf{d}\mathbf{U}} \mathbf{r} \quad (23)$$

and together with formula (21), this gives

$$\hat{\theta}_{LS} = (\mathbf{d}^T \mathbf{d})^{-1} \mathbf{d}^T E_{\mathbf{d}\mathbf{U}} \mathbf{r} = (\mathbf{d}^T \mathbf{d})^{-1} \mathbf{d}^T \mathbf{d} (\mathbf{d}^\perp P_{\mathbf{U}}^\perp \mathbf{d})^{-1} \mathbf{d}^\perp P_{\mathbf{U}}^\perp \mathbf{r} = \frac{\mathbf{d}^T P_{\mathbf{U}}^\perp \mathbf{r}}{\mathbf{d}^T P_{\mathbf{U}}^\perp \mathbf{d}}$$

This is yet another confirmation that the OSP detector is equivalent to the least squares estimator of θ in the model (1). In [1], a detector called an oblique subspace projection classifier (OBC) is defined as

$$D_{OBC}(\mathbf{r}) = \mathbf{d}^T E_{\mathbf{d}\mathbf{U}} \mathbf{r}$$

From (23), OBC is proportional to $\hat{\theta}_{LS}$, which is the same as the OSP detector. In [6] (Section 8.2.3), another version of the oblique projection detector is defined with additional scaling, which again is equivalent to OSP.

In [1], a detector called a signature space orthogonal projection classifier (SSC) is defined as

$$D_{SSC}(\mathbf{r}) = \mathbf{d}^T P_{\mathbf{U}}^\perp P_{\mathbf{M}} \mathbf{r} \quad (24)$$

From (22),

$$D_{SSC}(\mathbf{r}) = \mathbf{d}^T P_{\mathbf{U}}^\perp (\mathbf{d} \cdot \hat{\theta}_{LS} + \mathbf{U} \cdot \hat{\gamma}_{LS}) = \mathbf{d}^T P_{\mathbf{U}}^\perp \mathbf{d} \cdot \hat{\theta}_{LS},$$

which means that the SSC detector is another scaled version of the least squares estimator and the OSP detector. This also shows that

$$D_{SSC}(\mathbf{r}) = \mathbf{d}^T P_U^\perp \mathbf{r}$$

which is the same as the originally defined (see [7]) OSP detector (also called an *a priori* OSP detector ([1], [6])). In [5], a detector called the least squares orthogonal subspace projection (LSOSP) is defined using exactly the same definition as SSC in (24) (see formula (30) in [5]). This means that LSOSP is equivalent to SSC and OSP.

C. Details on the data downloaded from the USGS spectroscopy lab

The three reflectance spectra representing barite, chalcopyrite, and pyrite were downloaded from the USGS spectroscopy lab (<http://pubs.usgs.gov/of/2003/ofr-03-395/datatable.html>). The barite file is identified as “Barite HS79.3B W1R1Bb AREF,” chalcopyrite as “Chalcopyrite S26-36 W1R1Bb AREF,” and pyrite as “Pyrite S142-1 W1R1Bc AREF.” We used only wavelengths between 0.4 and 1.8 μm and further reduced the data set to 88 spectral bands by taking every fourth band. The three spectra are plotted in Figure 3 in the paper [10] (“chalpy” represents chalcopyrite, and the chalcopyrite and pyrite labels were inadvertently switched [13]).

Acknowledgments

The author would like to thank Prof. Chein-I Chang for providing the spectral data used in Table 2, and Steven Johnson for providing information about the barite, chalcopyrite, and pyrite spectra used in his paper [10]. The author is also grateful to anonymous reviewers, who pointed out weaknesses of a previous version of this paper, which led to significant improvements in the presented results.

Peter Bajorski received the B.S./M.S. degrees in mathematics from the University of Wroclaw, Poland, in 1982, and the Ph.D. degree in mathematical statistics from the Technical University of Wroclaw, Poland, in 1990. He held

positions at Cornell University, the University of British Columbia, Simon Fraser University, and NY State Department of Transportation. Currently, he is Associate Professor in the Graduate Statistics Department at the Rochester Institute of Technology. His research interests in remote sensing include target detection and unmixing in hyperspectral images. Other interests include multivariate statistical methods, regression techniques, and design of experiments. Dr. Bajorski has received several awards for his contributions to research and teaching. He has served as a referee for five scientific journals and has written numerous book reviews for book publishers and for professional journals. He is President of the Rochester Chapter of the American Statistical Association. Dr. Bajorski is a member of ASA, SPIE, and IEEE.

REFERENCES

1. C.-I. Chang, X.-L. Zhao, M. L. G. Althouse, and J. J. Pan, "Least squares subspace projection approach to mixed pixel classification for hyperspectral images," *IEEE Trans. Geosci. Remote Sensing*, vol. 36, pp. 898–912, May 1998.
2. D. Manolakis and G. Shaw, "Detection algorithms for hyperspectral imaging applications," *IEEE Signal Processing Magazine*, 19(1):29-43, January 2002.
3. L.L. Scharf, B. Friedlander, "Matched Subspace Detectors," *IEEE Trans. Signal Processing*, vol. 42, No. 8, pp. 2146–2156, August 1994.
4. S. Johnson, "The relationship between the matched filter operator and the target signature space orthogonal projection classifier," *IEEE Trans. Geosci. Remote Sensing*, vol. 38, pp. 283–286, Jan. 2000.
5. T. M. Tu, C.-H. Chen, and C.-I Chang, "A least squares orthogonal subspace projection approach to desired signature extraction and detection," *IEEE Trans. Geosci. Remote Sensing*, vol. 35, pp. 127–139, Jan. 1997.
6. C.-I. Chang, *Hyperspectral Imaging: Techniques for Spectral Detection and Classification*, Kluwer Academic/Plenum Publishers, 2003.
7. J. Harsanyi and C.-I Chang, "Hyperspectral image classification and dimensionality reduction: An orthogonal subspace projection approach," *IEEE Trans. Geosci. Remote Sensing*, vol. 32, pp. 779–785, July 1994.
8. J. J. Settle, "On the relationship between spectral unmixing and subspace projection," *IEEE Trans. Geosci. Remote Sensing*, vol. 34, pp. 1045–1046, July 1996.
9. R. T. Behrens and L. L. Scharf, "Signal processing applications of oblique projections operators," *IEEE Trans. Signal Processing*, vol. 42, pp. 1413–1423, June 1994.
10. S. Johnson, "Constrained energy minimization and the target-constrained interference-minimization filter," *Optical Engineering*, vol. 42, No. 6, pp. 1850–54, June 2003.
11. N.R. Draper and H. Smith, *Applied Regression Analysis*, John Wiley & Sons, 1998.
12. S. Johnson, "The Constrained Signal Detector," *IEEE Trans. Geosci. Remote Sensing*, vol. 40, pp. 1326–1337, June 2002.
13. S. Johnson, Personal communication.

14. C.-I. Chang, "Orthogonal Subspace Projection (OSP) Revisited: A Comprehensive Study and Analysis" *IEEE Trans. Geosci. Remote Sensing*, vol. 43, pp. 502–518, March 2005.
15. C. Chang, J. Liu, B. Chieu, H. Ren, C. Wang, C. Lo, P. Chung, C. Yang, and D. Ma, "Generalized constrained energy minimization approach to subpixel target detection for multispectral imagery," *Opt. Eng.* Vol. 39(5), pp. 1275–1281, 2000.
16. H. Ren and C. Chang, "Target-constrained interference-minimized approach to subpixel target detection for hyperspectral images," *Opt. Eng.* Vol. 39(12), pp. 3138–3145, 2000.
17. A. Ben-David and H. Ren, "Comparison between orthogonal subspace projection and background subtraction techniques applied to remote-sensing data," *Applied Optics*, Volume 44, Issue 18, 3846-3855, June 2005.

Table 1. The equivalent forms of the MFD and OSP detectors

Name	Equivalent Name	Defining Equation	Source explaining the equivalency
MFD	TSC	$D_{TSC}(\mathbf{r}) = \mathbf{d}^T P_U^\perp P_d \mathbf{r}$	[4]
OSP	SSC (or LSOSP)	$D_{SSC}(\mathbf{r}) = \mathbf{d}^T P_U^\perp P_M \mathbf{r}$	Appendix Section VI.b
	OBC	$D_{OBC}(\mathbf{r}) = \mathbf{d}^T E_{du} \mathbf{r}$	Appendix Section VI.b

Table 2. Above diagonal: angles ω (in degrees) between spectra of five materials used in Example 1. Below diagonal: Signal to Background Ratio $SBR(\mathbf{d}, \mathbf{u}_i)$ where \mathbf{d} is in rows and \mathbf{u}_i in columns. The values in parentheses next to the material names are the Euclidian norms $\sqrt{\mathbf{d}^T \mathbf{d}}$.

	blackbrush	creosote leaves	dry grass	red soil	sagebrush
blackbrush (3.11)		10.1	14.8	23.3	3.9
creosote leaves (4.45)	1.43		24.1	32.7	7.4
dry grass (6.55)	2.10	1.47		12.5	17.0
red soil (5.09)	1.64	1.14	0.78		25.9
sagebrush (4.60)	1.48	1.03	0.70	0.90	

Table 3. Efficiency of the MFD with respect to the OSP as defined in (11) and calculated according to (18) for the five materials used in Example 1.

	Blackbrush	creosote leaves	dry grass	red soil	sagebrush
blackbrush		-2.31	-4.06	-1.27	-6.97
creosote leaves	1.77		-0.84	0.07	-0.20
dry grass	2.12	0.93		1.11	1.12
red soil	1.11	0.49	-1.18		0.43
sagebrush	4.77	0.32	-1.24	0.01	

Table 4. Above diagonal: angles ω (in degrees) between spectra of three materials used in Example 2. Below diagonal: Signal to Background Ratio $SBR(\mathbf{d}, \mathbf{u}_i)$ where \mathbf{d} is in rows and \mathbf{u}_i in columns. The values in parentheses next to the material names are the Euclidian norms $\sqrt{\mathbf{d}^T \mathbf{d}}$.

	barite	chalcopyrite	pyrite
barite (5.98)		11.9	7.3
chalcopyrite (0.56)	0.09		12.3
pyrite (0.95)	0.16	1.71	

Table 5. Efficiency of the MFD with respect to the OSP as defined in (11) and calculated according to (18) for the three materials used in Example 2.

	Barite	chalcopyrite	pyrite
barite		4.40	6.59
chalcopyrite	-45.83		-3.14
pyrite	-40.84	2.01	

Figure 1. The line of equality between the power of the OSP and the MFD detectors (for a one-dimensional background) in the system of coordinates of $SBR(\mathbf{d}, \mathbf{u}_1)$ on the vertical axis and the angle ω on the horizontal axis. The MFD performs better than the OSP for cases above the line, and worse than the OSP for those below the line.

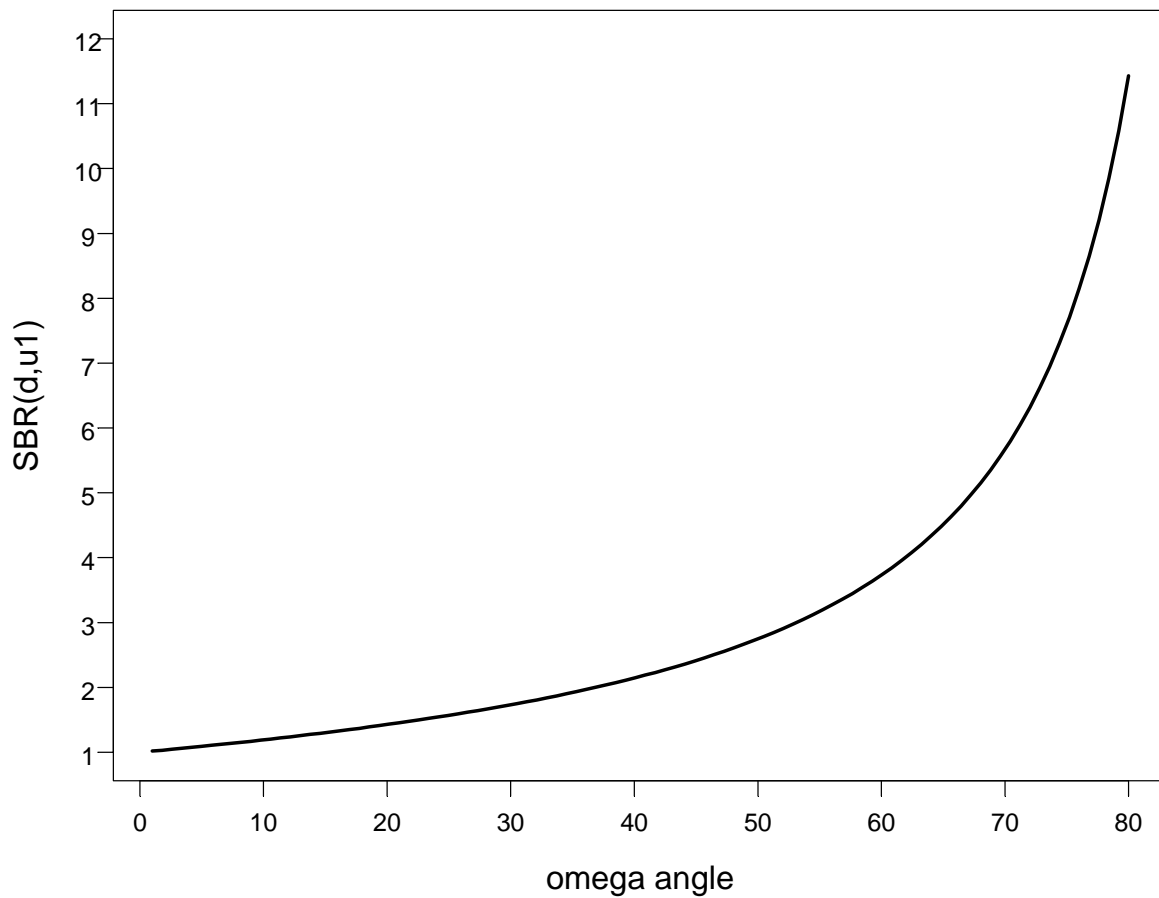


Figure 2. Power curves for the OSP (solid line) and MFD (dashed line) detectors as functions of the SNR parameter B ($\alpha = 0.001$) when the dry grass spectrum is the target \mathbf{d} and the creosote leaves spectrum is the background \mathbf{u}_1 (Example 1).

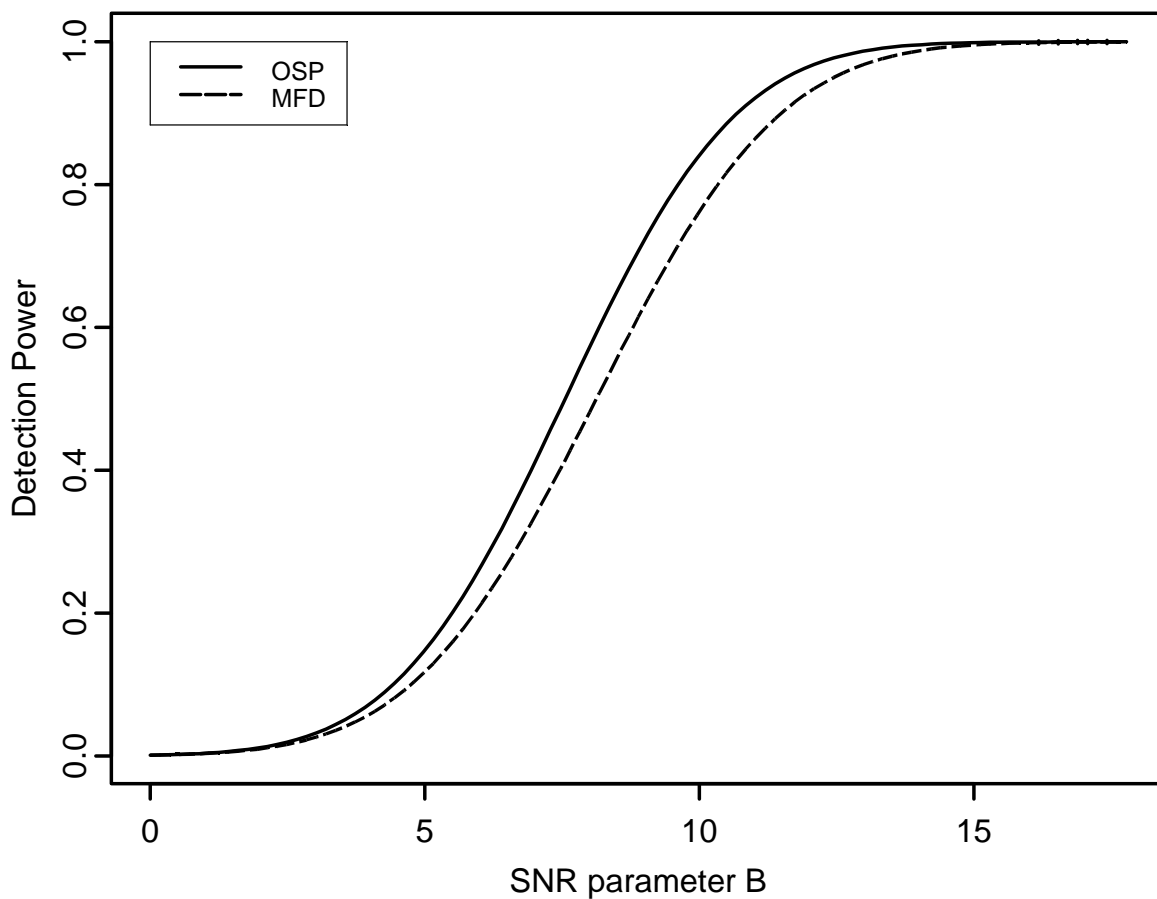


Figure 3. Power curves for the OSP (solid line) and MFD (dashed line) detectors as functions of the SNR parameter B ($\alpha = 0.001$) when the red soil spectrum is the target \mathbf{d} and the creosote leaves spectrum is the background \mathbf{u}_1 (Example 1).

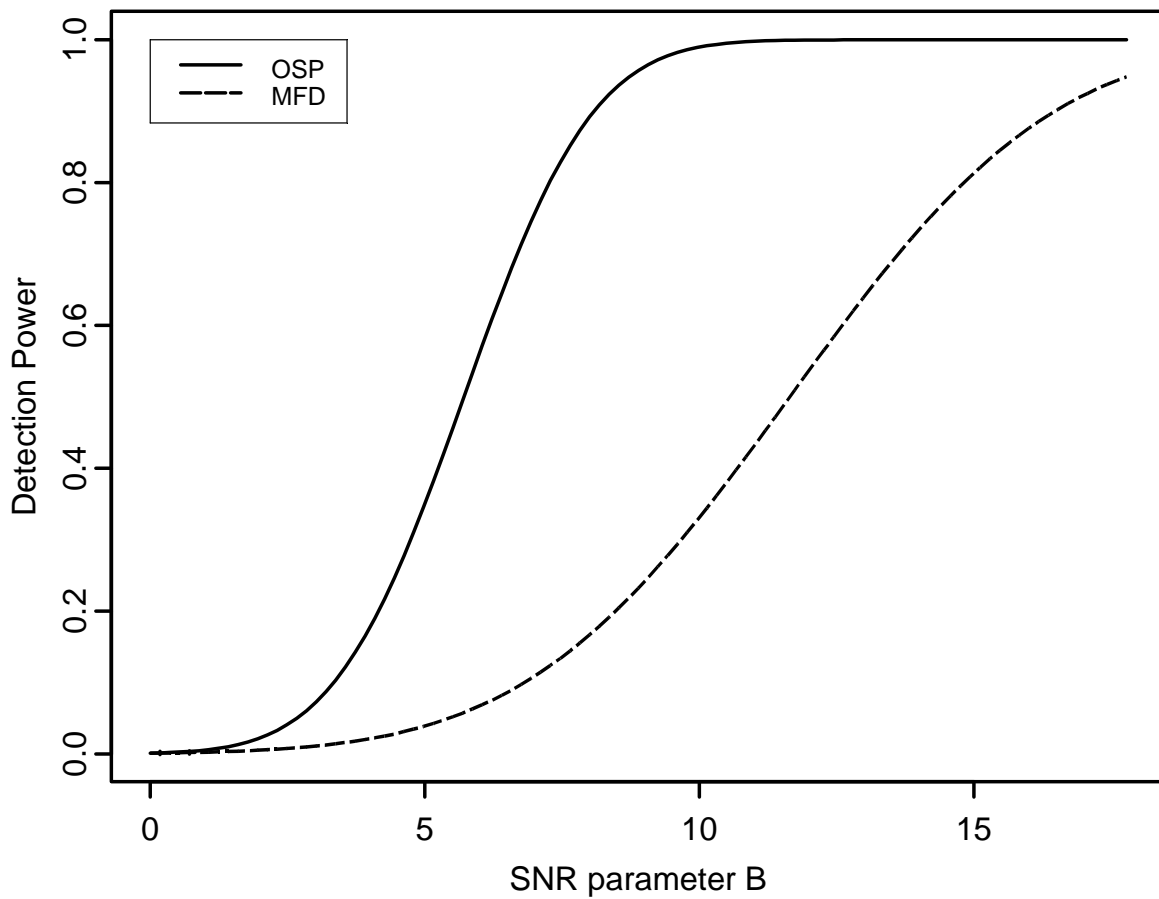


Figure 4. Power curves for the OSP (solid line) and MFD (dashed line) detectors as functions of the SNR parameter B ($\alpha = 0.001$) when the pyrite spectrum is the target \mathbf{d} and the chalcopyrite spectrum is the background \mathbf{u}_1 (Example 2).

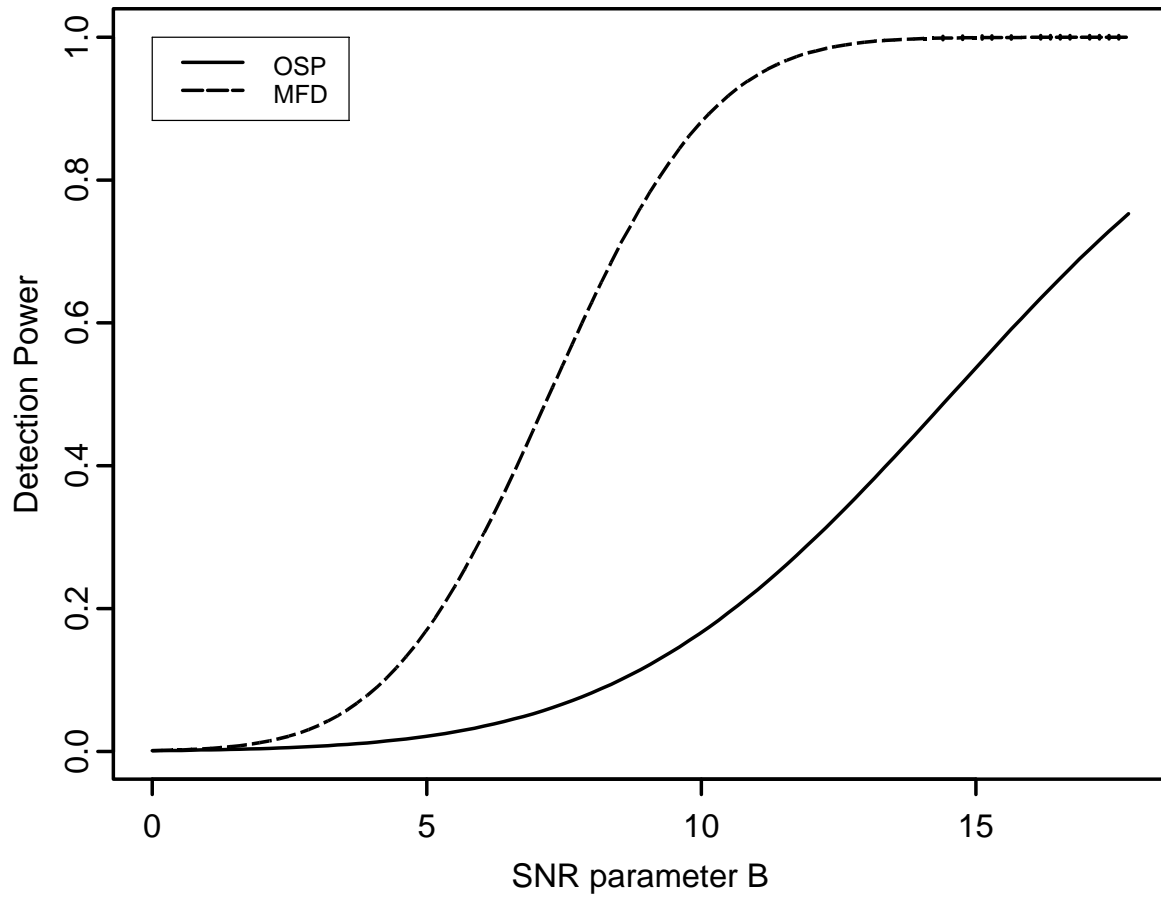


Figure 5. The detection power of the MFD ($\alpha = 0.001$, $\theta = 0.1$) as a function of the abundance s at various levels of t . The first (solid) line on the left-hand side is for $t = 0.1$ and the subsequent lines are for t increasing by 0.1 until the last line on the right-hand side (function) for $t = 0.9$.

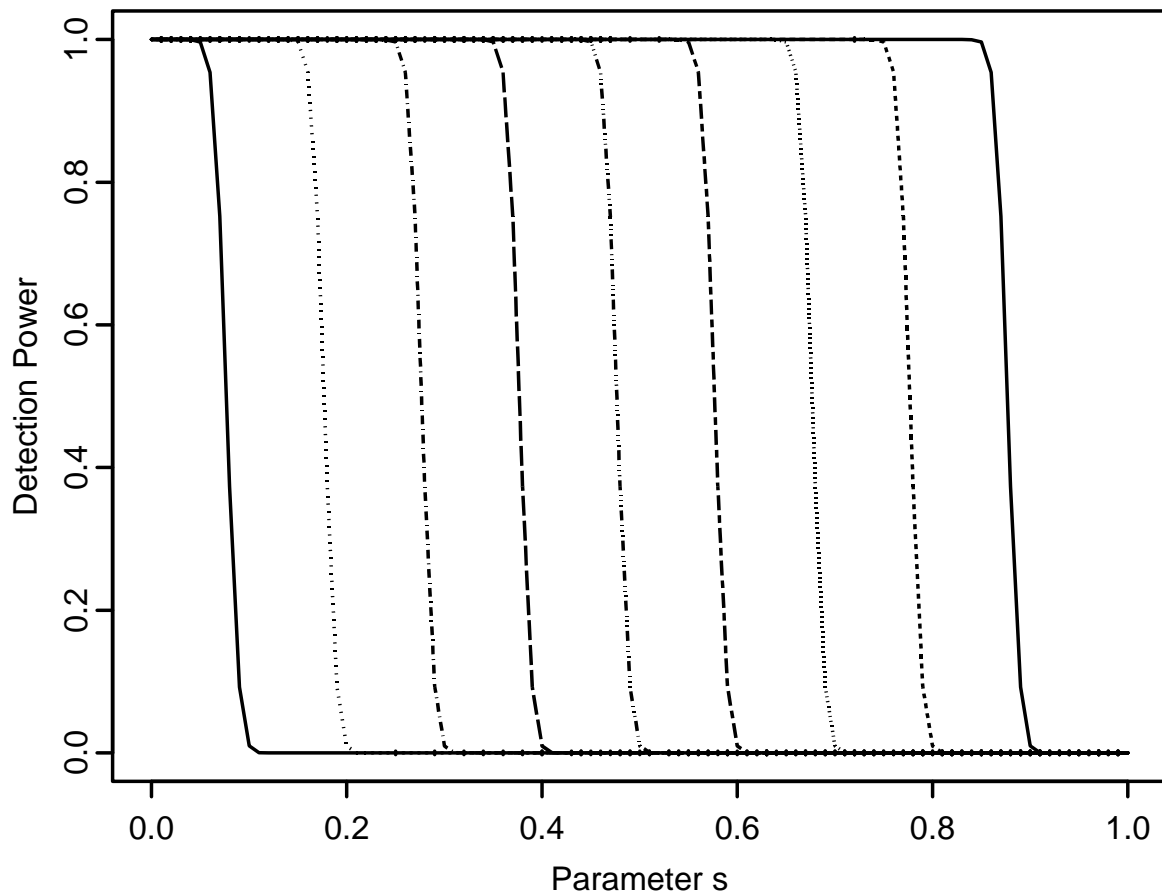


Figure 6. The detection power of the OSP (solid line) and the lower limit of the MFD power (dashed line), that is, the right-hand side of (19), as functions of the parameter θ ($\alpha = 0.001$).

